Brodogradnja Volume 75, Number 3 (2024) 75303

journal homepage: www.brodogradnja.fsb.hr

Brodogradnja

An International Journal of Naval Architecture and Ocean Engineering for Research and Development

Optimization of exhaust ejector with lobed nozzle for marine gas turbine

Hong Shi[*1], *Rui Wang*[1], *Yinglong Xiao*[2], *Xiaojian Zhu*[2], *Rentong Zheng*[1], *Caiyue Song*[1], *Zhenrong Liu*[1]

[1] *College of Energy & Power Engineering, Jiangsu University of Science and Technology, Zhenjiang 212000, China*
[2] *Shanghai Marine Diesel Engine Research Institute, 3111 Huaning, Minhang, Shanghai 201108, China*

ARTICLE INFO

Editor-in-Chief: Prof. Nastia Degiuli
Associate Editor: PhD Ivana Martić

Keywords:
Marine gas turbine
Lobed nozzle ejector
Ejecting cooling performance
Orthogonal test
CRITIC method

ABSTRACT

To attain high-performance ejector configurations, an ejection characteristic testing system was established initially to validate the reliability of the Realizable k-ε turbulent model. Subsequently, optimization investigations were conducted on lobed nozzle ejectors with various structural parameters. The effects of four key structural parameters, including lobed nozzle expansion angle α, lobed nozzle width d, number of lobes in the nozzle n, and height of the square-to-circle section h, were systematically studied. Furthermore, the CRITIC method was employed for multi-objective evaluation to identify the optimal design configuration for the casing ejector. The research findings revealed that among the structural parameters, the lobed nozzle expansion angle α exerted the greatest influence on the ejection coefficient and pressure loss coefficient. The weights of the evaluation criteria were determined by the CRITIC method as follows: ejection coefficient (49.38%) < pressure loss coefficient (50.62%). The optimal design configuration determined by the CRITIC method included $\alpha = 45°$, $d = 150$ mm, $n = 14$, and $h = 600$ mm. The resulting enclosure design ensures smooth airflow within the system, preventing the backflow of high-temperature mainstream fluid and heating the enclosure. It also maintains a temperature distribution in the typical cross-section that meets specified requirements. Additionally, it facilitates improved mixing of mainstream and secondary fluid and reduces exhaust gas temperature.

1. Introduction

Gas turbines are widely used in the maritime industry as efficient, energy-saving and environmentally friendly power systems [1]. Enclosing gas turbines in a casing is a common practice to control engine temperature and ensure safe operation [2]. In a gas turbine, compressed air enters the combustion chamber for combustion and then drives the generator or propeller through a turbine. During this process, the gas temperature is extremely high, requiring cooling to maintain normal turbine operation [3,4]. Additionally, placing the gas turbine in a sealed casing results in elevated temperatures inside the casing due to heat dissipation from the turbine unit and slight gas leaks from components such as gas pipes and flanges [5]. These

* Corresponding author.
E-mail address: shihong@nuaa.edu.cn

http://dx.doi.org/10.21278/brod75303
Submitted 21.02.2024; Accepted 03.05.2024.
ISSN 0007-215X; eISSN 1845-5859

elevated temperatures adversely affect the efficiency of the gas turbine. The casing also contains fire detection systems, fire suppression systems, lighting systems, pipelines, and electrical instruments. Improper temperature control of the casing can cause secondary heating of auxiliary equipment through radiative heat transfer from the high-temperature surfaces of the gas turbine unit, leading to secondary damage and potential risks to external personnel. Therefore, proper ventilation and cooling of the casing are crucial [6]. Injection cooling is a commonly used cooling method that utilizes exhaust gas expelled from the gas turbine's exhaust diffuser to extract gas from inside the casing [7-9]. The effectiveness of injection cooling is influenced by various factors, including the structural parameters of the main jet nozzle, the shape and size of the mixing duct, and their compatibility [10]. Accurate evaluation of the performance of injection cooling requires comprehensive consideration of these influencing factors and an in-depth understanding of their impact. Only through thorough research can well-designed injection cooling devices, matched with gas turbine power, be developed to enhance gas turbine performance. Therefore, in-depth research and optimization of injection cooling devices hold significant importance for the development of high-power marine gas turbines, providing technical foundation. Currently, researchers have conducted experimental and numerical simulation studies on the injection cooling mechanism of casings [11].

Vahidi et al. [12] employed forced ventilation and combined it with CFD numerical simulations to identify potential gas leakage areas within the casing and designed baffles to optimize the flow field. An experimental model was also established to validate the dilution of potential gas leakage areas inside the casing and ensure the desired temperature of both the casing interior and the casing itself. Lucherini et al. [13] used transparent organic glass for the shell and ventilation ducts of the experimental model to visualize the overall flow, facilitating the study of gas leakage. The research results demonstrated a high consistency between experimental and computational data, validating the accuracy and reliability of the CFD study conducted during the design phase. Kowalski et al. [14] chose two different methods to simulate forced ventilation and compared them with experimental data. The results indicated that using two independent outward momentum sources better matched the experimental results, with gas leakage areas primarily concentrated around the engine section. In terms of ejector structural design and optimization, Birk and Davis [15] studied the marine multi-stage exhaust ejector system and designed ejectors named DRES Ball with a central body and E/D with four nozzle ejectors. These devices were used to reduce infrared radiation in Canadian frigates and destroyers. Maqsood and Birk [16,17] conducted numerical and experimental research on curved ejectors, indicating that the ejection rate initially decreases and then increases with increasing curvature angle. Increasing the swirl angle can enhance the ejection rate but leads to pressure losses, suggesting the existence of an optimal swirl angle. Subsequently, based on their previous study, Maqsood and Birk [18] installed an ejector-style diffuser at the rear of the ejector and investigated its impact on the ejection performance. The results demonstrated that the ejector-style diffuser significantly improved the ejection performance for highly curved ejectors. In a study conducted in 2017, Maqsood et al. [19] explored the effectiveness of curved elliptical ejectors as infrared signature suppressors, noting that the curvature and swirl of the ejector increased the wall temperature. Hu et al. [20-22] revealed that rapid mixing occurred between the mainstream fluid and the ejected fluid at a distance of 2 times the nozzle diameter, resulting in intense mixing phenomena. Nastase [23] compared the ejection capabilities of two types of lobed nozzles, one without inclination and one with inclination, with a circular nozzle of the same outlet area and volume flow rate. The research results indicated that the lobed nozzle without inclination already exhibited superior ejection capabilities compared to the circular nozzle, and when inclinations were added internally and externally, the ejection flow rate of the lobed nozzle could reach four times that of the circular nozzle. Paul et al. [24] investigated the subsonic jet characteristics of a lobed ejector through numerical simulations and examined the effects of lobe length, lobe penetration, and lobe count on the injection performance. The study revealed that the centerline velocity decay of the lobed nozzle was significantly faster compared to the Chevron nozzle, with peak Reynolds stresses occurring near the nozzle exit. Sheng et al. [25] and Liu et al. [26] studied the effects of the spoilers on the injection coefficient, total pressure loss, mixing efficiency, and temperature of the mixing duct wall. Their research indicated that the impingement of the primary stream on the mixing duct was observed to depress mixing in the region off the lobe peaks and decrease the pumping ratio and total pressure recovery coefficient. Chevron spoilers located at lobe peaks can increase the spacing between the lobe peaks and the mixing duct and deflect the flow

direction of the primary stream off the lobe peaks, thereby suppressing impingement of the primary stream on the mixing duct. Sheng et al. [27] used numerical simulation to investigate the jet mixings of different constructional lobed mixers comprised of lobed nozzles with and without a mixing duct. Their research indicated that increasing the lobe angle can cause high-temperature mainstream oblique impact on the mixing duct wall, which is not conducive to reducing the temperature of the mixing duct wall.

In summary, the ejector of the engine casing has become a widely studied subject for scholars both domestically and internationally, involving multiple aspects of investigation. Scholars have conducted in-depth research on the ejection mechanism of casing ejectors and made significant efforts in optimizing the lobed structure [28]. However, there are still some unresolved issues. Firstly, there is no consensus on the evaluation criteria for casing ejectors, which requires further exploration and discussion. Secondly, existing studies on ejector performance mainly focus on the infrared suppressor [29-31] at the outlet of the power device, with relatively limited research on the optimization of ejectors coupled with casing structures. Therefore, in future research, it is necessary to address these issues to promote the development of the engine casing field.

Based on this, this study conducts a systematic performance evaluation by introducing multiple objective evaluation indicators such as ejection coefficient (EC), pressure loss coefficient (PLC) and temperature metric. Furthermore, the key factors that significantly affect the ejection performance, such as lobed nozzle expansion angle α, lobed nozzle width d, number of the lobed nozzle n and height of the square-to-circle section h, are identified and studied through orthogonal experiments to analyse the system performance under orthogonal parameters. Further, an optimal casing configuration is determined through multi-objective evaluation, and the typical temperature distribution of the selected scheme is verified to meet the design requirements.

2. Geometry and method

2.1 Physical model and boundary condition

The ejecting cooling system of a marine gas turbine is examined and a physical model is established as shown in Fig. 1.

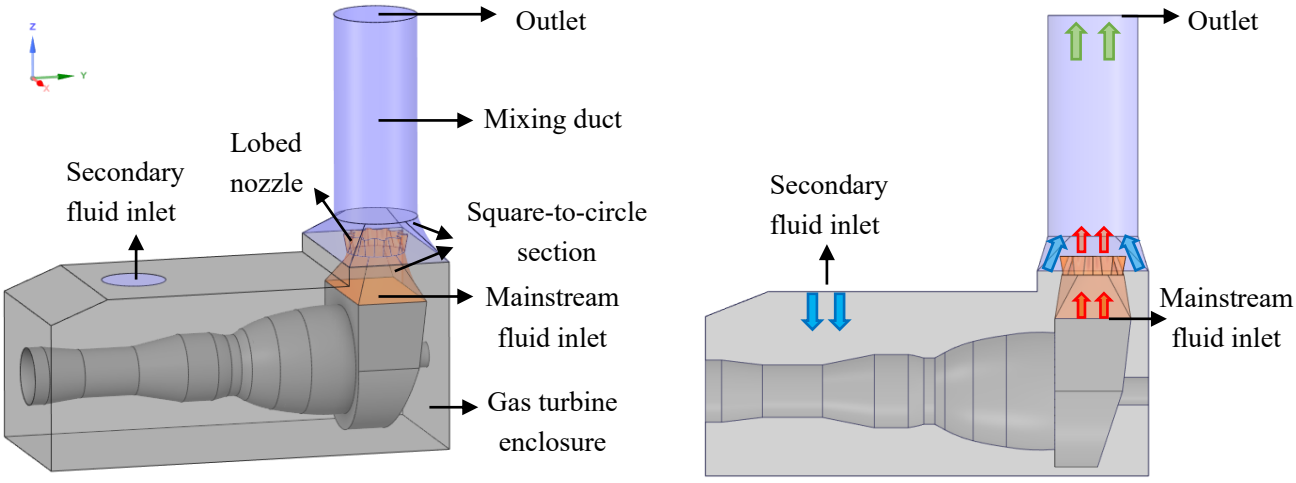

(a) Definition of structure (b) Definition of outlet and inlet

Fig. 1 Physical model

As shown in Fig. 1, an exhaust ejector with a lobed nozzle ejector in the gas turbine enclosure is investigated in this study [28]. Since the exhaust plenum outlet is square, a square-to-circle transition section is needed to connect the two parts of the exhaust plenum outlet and the lobed nozzle, and the same is true for the connection between the mixing tube and the gas turbine enclosure. The parameters of the ejector as shown in Fig. 2.

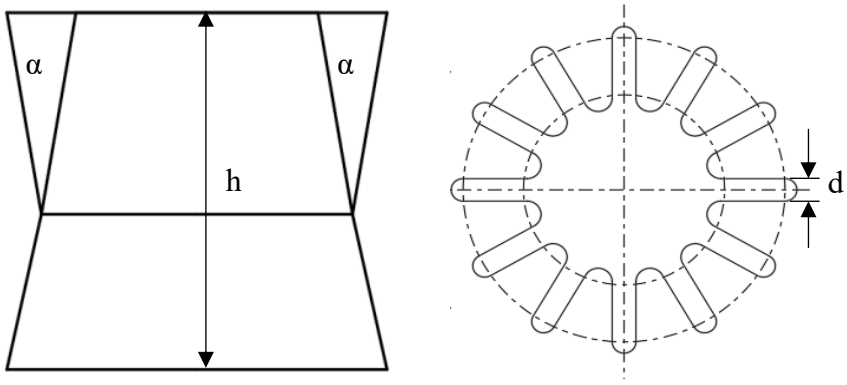

(a) Lobed nozzle ejector (b) Lobed nozzle ejector outlet profile

Fig. 2 Definition of structural parameters

The ejecting cooling system's aerodynamic characteristics are investigated using an ideal gas as the fluid medium. Considering the accuracy of the Realizable *k-ε* model in simulating round hole jet flows, this numerical simulation employs the Realizable *k-ε* turbulence model [28]. The strength of FLUENT in simulating turbulent lies in its provision of a multitude of advanced turbulence models and solution algorithms, coupled with its powerful parallel computing capabilities, which together ensure the precision and efficiency of the simulations. In this study, the pressure-based solver of FLUENT [32], with the coupling solution of velocity and pressure is achieved through the SIMPLE algorithm [33]. The inlet and outlet boundary conditions are specified as outlined in Table 1.

Table 1 Boundary conditions

Boundary name	Boundary types and parameter settings	
Mainstream fluid inlet (High-temperature gas)	Boundary type	Mass flow rate inlet
	Mass flow rate	31.4 kg/s
	Temperature	764 K
	Airflow direction	Normal
Secondary fluid inlet (Ambient air)	Boundary type	Pressure inlet
	Temperature	300 K
	Gauge pressure	0 Pa
	Airflow direction	Normal
Outlet (Blended gas)	Boundary type	Pressure outlet
	Temperature	300 K
	Gauge back pressure	1100 Pa

The gas turbine is divided as shown in Fig. 3, which is divided into 9 parts from left to right, numbered 1 ~ 9 in turn.

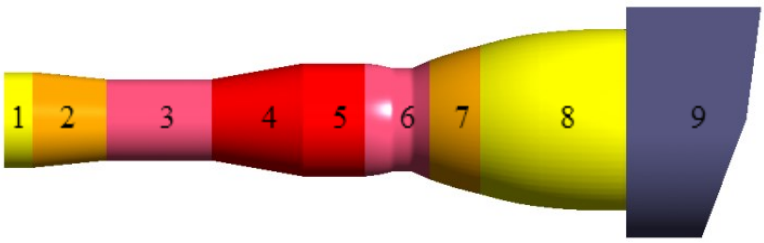

Fig. 3 Segment definition of gas turbine

Each part is set to a slip-free wall with an emissivity of 0.9 [28]. The temperature of each part is defined in sections according to the state of gas turbine operation, and the specific temperature settings are shown in Table 2.

Table 2 Specific temperature settings

Number	Name	Temperature	Number	Name	Temperature
1	Inlet section	350 K	2	Low pressure air compressor	477 K
3	High pressure air compressor	589 K	4	Combustion	661 K
5	Aft combustion chamber	661 K	6	Transition section	589 K
7	Power turbine	455 K	8	Aft power turbine	455 K
9	Exhaust plenum	439 K	—	—	—

2.2 Evaluation metrics

(1) Entrainment Coefficient (EC)

The EC coefficient is a dimensionless coefficient that indicates the suction capacity of the ejecting cooling system, and is defined as follows:

$$n = \frac{G_2}{G_1}, \tag{1}$$

where G_1 is the mass flow rate of the mainstream fluid, G_2 is the mass flow rate of the secondary fluid.

(2) Pressure Loss Coefficient (PLC)

The PLC is a dimensionless coefficient which indicates the pressure loss in the ejecting cooling system, and is expressed as follows:

$$\prod = \frac{P_{01} - P_{02}}{q}, \tag{2}$$

where P_{01} is the total pressure at the mainstream fluid inlet, P_{02} is the total pressure at the outlet of the mixing tube, q is the dynamic pressure at the mainstream fluid inlet.

(3) Temperature Indicator (TI)

The air temperature, represented by a typical section inside the gas turbine enclosure, should be below 82 °C (355 K) [34]. It is important to note that achieving a substantial reduction in the temperature of the immediate wall region is challenging solely through the application of cooling, owing to the elevated temperature of the gas turbine walls. Therefore, the monitoring range does not include temperatures in the area within 100 mm height of the gas turbine surface [28].

2.3 Validation of numerical simulation methods

To ensure the reliability of the numerical simulation algorithm presented in this investigation, we constructed an ejection characteristic testing system for experimentation, as shown in Fig. 4. The system comprises variable frequency centrifugal fan, flow control valve, rectification section, exhaust ejection section, velocity sensor, smoke generator, and control system, along with other ancillary devices. The enclosure of this system incorporates an exhaust ejector with a convergent nozzle ejector, as shown in Fig. 5.

As shown in Fig. 6, smoke was used as a visual medium in the experiment to facilitate the presentation and evaluation of the ejection phenomenon. The fan frequency was set to the value of 40 Hz, and a high-precision pitot tube anemometer was used to measure the velocity at the converging nozzle inlet and the mixing tube outlet. The distribution of measurement points at the mixing tube outlet is shown in Fig. 7, with each point measured three times. The experimental results are presented in Table 3.

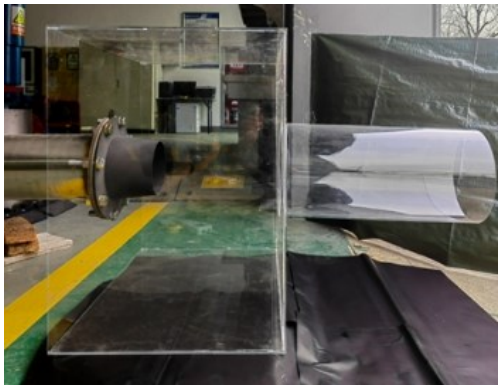

(a) Enclosure and ejector

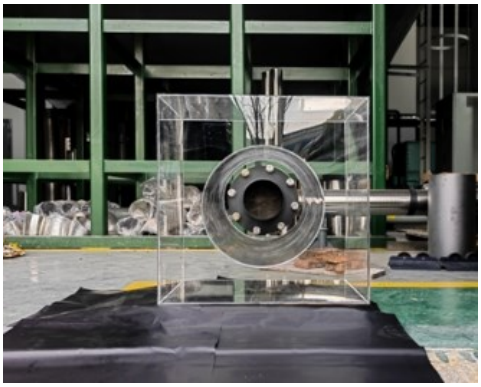

(b) Nozzle and mixing duct alignment

Fig. 4 Ejection characteristic testing system

Fig. 5 Convergent nozzle ejector

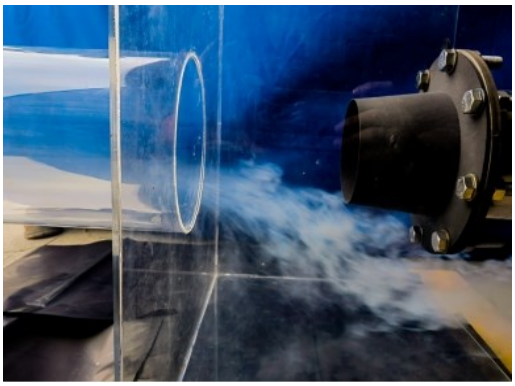

Fig. 6 Ejection phenomenon

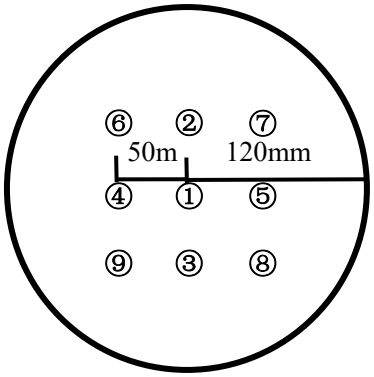

Fig. 7 Distribution of measuring points

Table 3 Experimental results

Fan frequency (Hz)	Average fan outlet velocity (m/s)	Point	1	2	3	4	5	6	7	8	9
40	22.57	Velocity (m/s)	32.08	26.11	25.93	29.67	28.39	27.87	23.37	25.38	27.16

Based on the exhaust ejection characteristic test mentioned above, models were created for the nozzle, inlet duct, mixing tube, and ground, maintaining the same dimensions and spatial relationships as in the experiment. The established model is shown in Fig. 8. Boundary conditions are the same as the experimental conditions. As shown in Fig. 8, except for the ground, the boundary conditions for all other surfaces in the computational domain were set as pressure-outlets, and Realizable k-ε turbulent model was used for simulation calculation. During the simulation, the airflow velocities at the test points were outputted, and the simulation

results were compared with the experimental results. The comparison between numerical simulation and experimental results is shown in Fig. 9.

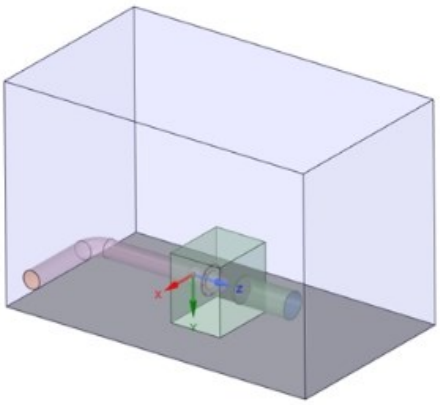

Fig. 8 Numerical simulation model

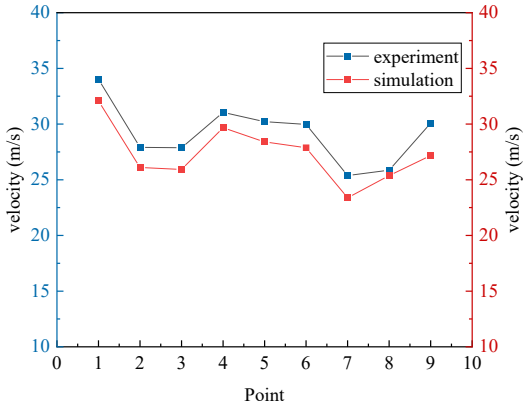

Fig. 9 Numerical simulation and experimental comparison results

From Fig. 9, it can be observed that the trend of the simulation results is generally consistent with the experimental results, with the absolute error rate of the four test points being 6.23%, remaining within 10%. Therefore, the Realizable *k*-*ε* turbulent model accurately predicts the actual velocity values, indicating that the Realizable *k*-*ε* turbulent model has a certain degree of reliability and can be used for the subsequent research.

2.4 Mesh independence verification

To ensure that the numerical simulation results are independent of the number of meshes, the original model is used here as an example, and five different sizes of meshes were set at 4.95 million, 6.45 million, 7.51 million, 8.42 million, and 9.77 million. Analyzing the effect of different mesh sizes on the results of numerical simulation, using the EC as an indicator as shown in Fig. 10.

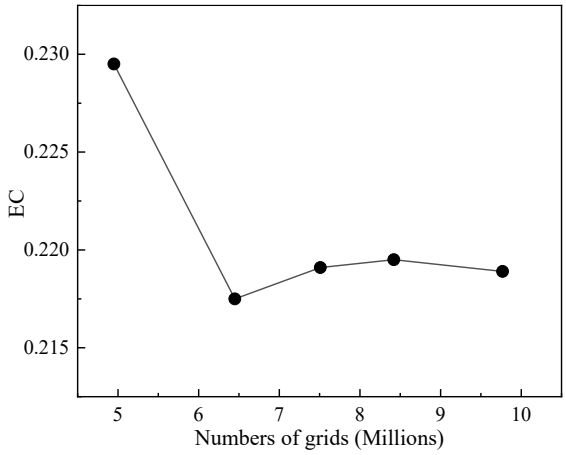

Fig. 10 Mesh independence numerical validation results

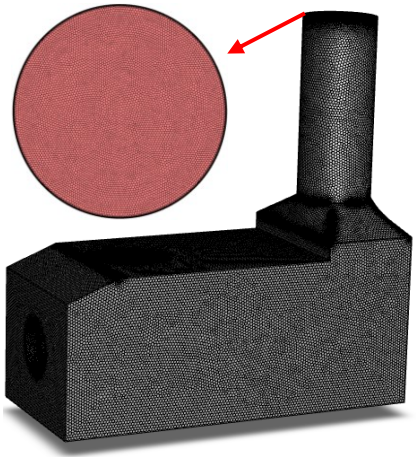

Fig. 11 Mesh and boundary Layer

It can be seen that the EC tends to stabilize when the mesh size exceeds 7.01 million, and there is no significant change as the mesh size increases further. Therefore, considering the mesh density and computational resources, we choose to set the mesh size to 7.01 million. Fig. 11 shows the mesh used in this study. We refined the mesh and boundary Layer in areas with significant flow fluctuations to ensure that the *y*+ range remained between 30 and 300 [35].

3. Numerical calculation results and analysis

3.1 Mechanistic study of lobed nozzle ejector

In this section, different lobed nozzle expansion angles α, lobed nozzle widths d, number of lobes n and heights of square-to-circle h of the lobed nozzle ejector will be compared and analyzed, and the mechanism of the ejector will be investigated and summarized.

3.1.1 Angle of lobed nozzle

This section conducts a comparative analysis of lobed nozzle ejector structures with adjusting expansion angles of α = 25°, 30°, 35°, 40°, and 45°. By keeping the outlet of the lobed nozzle unchanged and solely adjusting its height, the expansion angle was effectively altered. Other structural parameters are d = 120 mm, n = 10, and h = 630 mm. These configurations are presented in Fig. 12 and the numerical simulation outcomes corresponding to the different lobed nozzle angles are systematically compiled and displayed in Table 4 for comprehensive assessment and comparison.

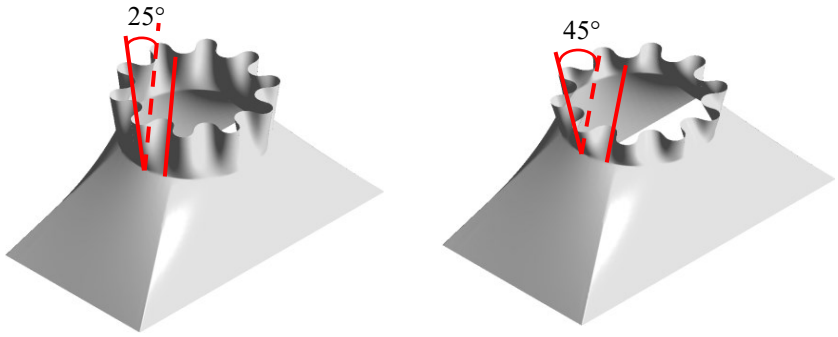

(a) α = 25° (b) α = 45°

Fig. 12 Exhaust ejector structure

Table 4 Numerical simulation results for different lobed nozzle angles

Structure	P_1 (Pa)	P_2 (Pa)	q (Pa)	EC	PLC
25°	2043.926	4246.129	210.919	0.1983	10.4410
30°	2059.712	4269.302	210.902	0.2191	10.4769
35°	2118.419	4622.414	210.226	0.2484	11.9110
40°	2141.619	4764.731	209.907	0.2657	12.4965
45°	2216.502	5170.030	209.108	0.2699	14.1244

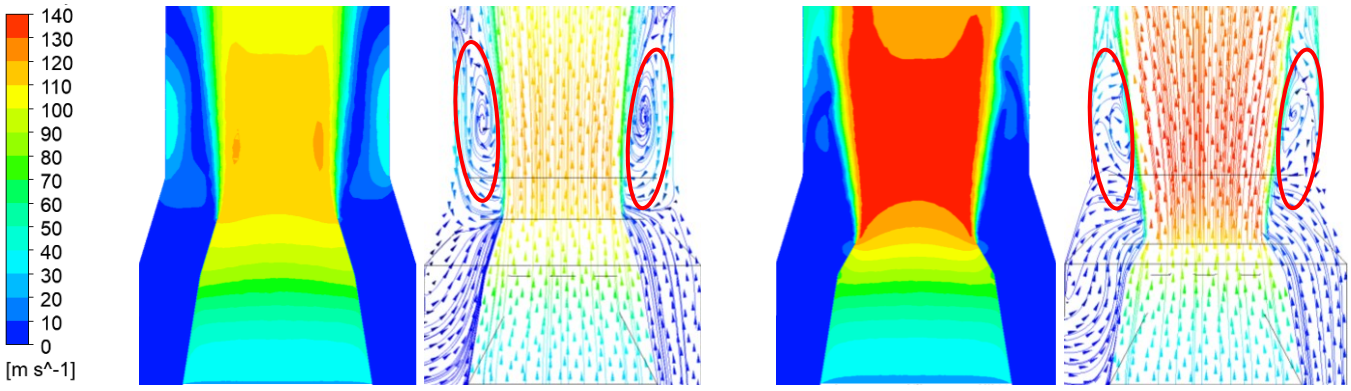

(a) α = 25° (b) α = 45°

Fig. 13 Velocity field of the mixing tube inlet section

As can be seen from Table 4, with the increase of the lobed nozzle angle α, the EC increases and the increase reaches 0.0716. The PLC gradually increases, with an increase of 3.6834, as the differential pressure

(P_2-P_1) increases and q decreases slightly. As the expansion angle of the lobed nozzle is adjusted by lifting and lowering the nozzle outlet surface, when the expansion angle increases, the leaf nozzle trough is concave inwards, further compressing the flow area of the mainstream fluid, which will lead to an increase in the mainstream velocity, as shown in Fig. 13.From Fig. 13, as the α increases, the mainstream flow velocity also increases, and the entrainment ability is enhanced. The increase in the secondary stream flow rate causes the low-speed recirculation area in the mixing duct to be weakened and destroyed, this phenomenon was also confirmed in the study by Shi et al [28]. Therefore, the EC increases significantly.

As the intensification of the inward concavity of the lobed nozzle trough leads to an increase in the internal drag loss of the ejector, as shown in Fig. 14, so (P_2-P_1) increases and PLC decreases.

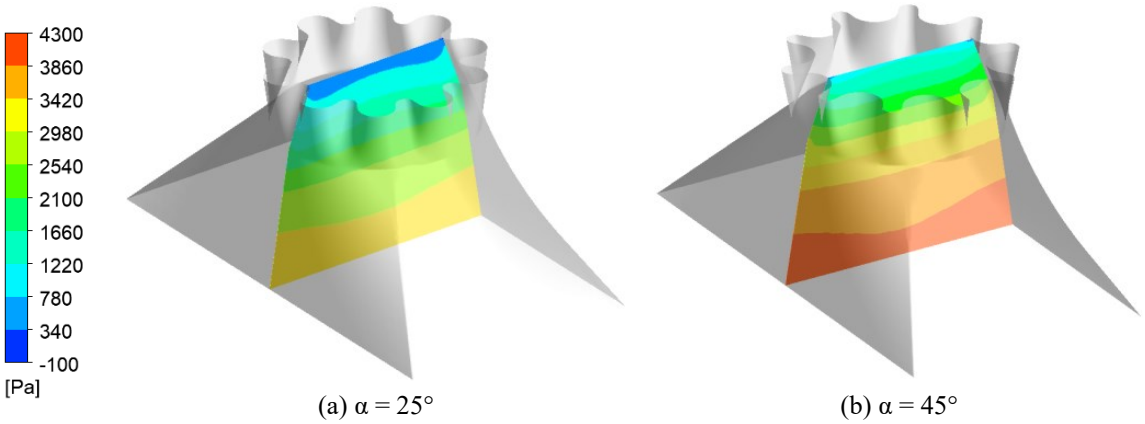

(a) α = 25° (b) α = 45°

Fig. 14 Pressure distributions inside the lobed nozzle

The temperature around the ejector outlet changes sharply, and observing the temperature distribution can provide further understanding of the mixing of the flows. The temperature distribution of the mixing tube inlet section as shown in Fig. 15.

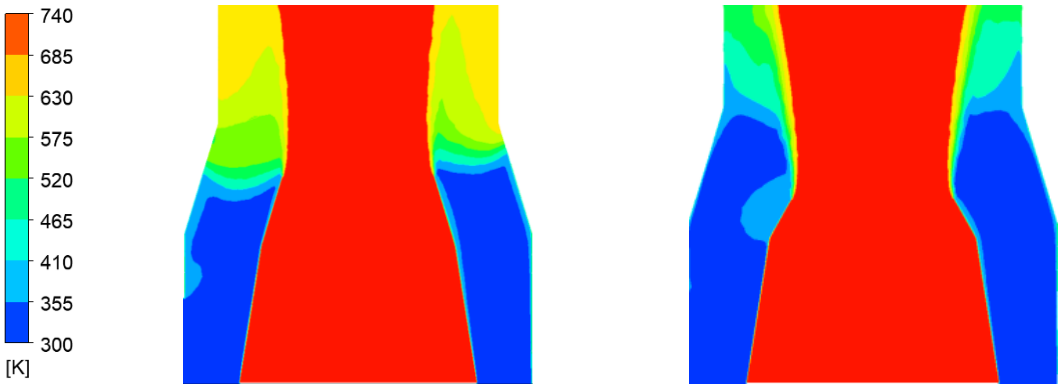

(a) α = 25° (b) α = 45°

Fig. 15 Temperature distributions of the mixing tube inlet section

As can be seen from Fig. 15, the vortex structure in the mixing tube wall region will absorb the mainstream temperature and transfer to the enclosure, restricted flow passage will result in inadequate heat dissipation within the wall region of the enclosure, and too large an expansion angle will increase the angle of the wave peaks and valleys of the exit jets. This increases the contact area of the mainstream with the secondary fluid, better blend to the mainstream, so that too large a lobe nozzle angle will be made to the outside of the valley of the wave of the small temperature increase.

3.1.2 The width of the lobed nozzle

In this section, we compare and analyzed different widths d of the lobed nozzle ejector. The lobed nozzle ejector with d = 80 mm, 100 mm, 120 mm, 140 mm, and 160 mm are compared. Other structural parameters are α = 30°, n = 10, and h = 630 mm. The numerical simulation results for different lobed nozzle widths are shown in Table 5.

Table 5 Numerical simulation results for different lobed nozzle widths

Structure	P_1 (Pa)	P_2 (Pa)	q (Pa)	EC	PLC
80 mm	2179.157	4933.634	209.569	0.2543	13.1435
100 mm	2118.857	4582.858	210.259	0.2299	11.7189
120 mm	2059.712	4269.302	210.902	0.2191	10.4769
140 mm	2029.192	4142.006	211.141	0.2133	10.0066
160 mm	2032.458	4069.025	211.284	0.2059	9.6390

As can be seen from Table 5, the EC decreases from 0.2543 to 0.2059 with the increase of the lobe nozzle width d. When the P_2 decreases significantly, pressure difference between inlet and outlet (P_2-P_1) decreases, and q increases slightly, resulting in the PLC decreasing from 13.1435 to 9.639. The adjustment of the width of the lobed nozzle will directly affect the mixing area of the main and secondary streams, when d is increased from 80 mm to 160 mm, the main stream recirculation area increases significantly, while the secondary stream recirculation area decreases. The location where the secondary stream decreases is the location of the trough, as shown in Fig. 16. This is similar to the conclusion of reference [36]. When d increases, the recirculation area of the secondary flow decreases and the EC decreases significantly.

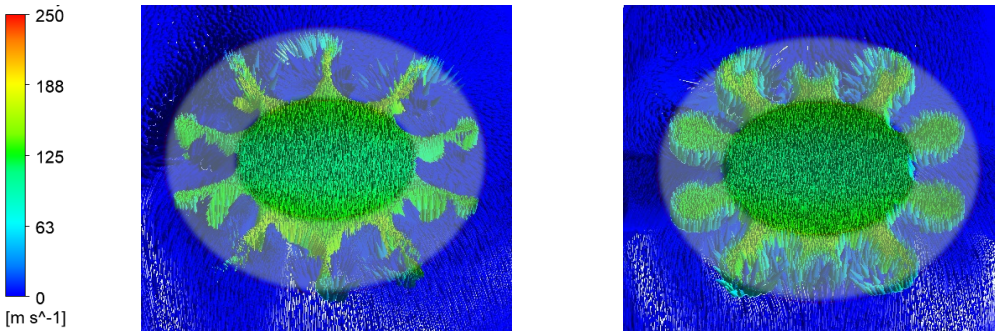

(a) d = 80 mm (b) d = 160 mm

Fig. 16 Velocity vector field at the outlet of the ejector

While increasing the main stream outflow area will reduce the resistance loss of the main stream inside the inducer, and at the same time reduce the flow velocity. Therefore, the total pressure at the outlet decreases significantly, as shown in Fig. 17, and the PLC decreases accordingly.

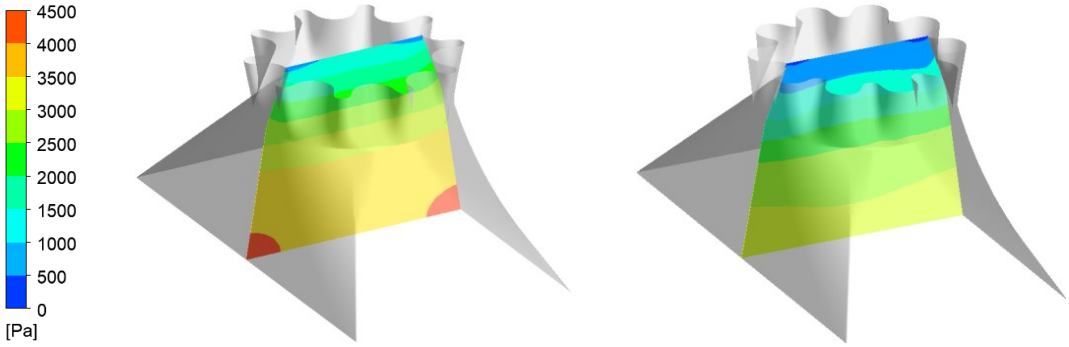

(a) d = 80 mm (b) d = 160 mm

Fig. 17 Pressure distributions inside the lobed nozzle

As the width of the lobed nozzle increases, the temperature in the nozzle outlet-mixing tube inlet region decreases, most noticeably on the right side, and the heating effect of the high-temperature main stream on the chamber will diminish, as shown in Fig. 18.

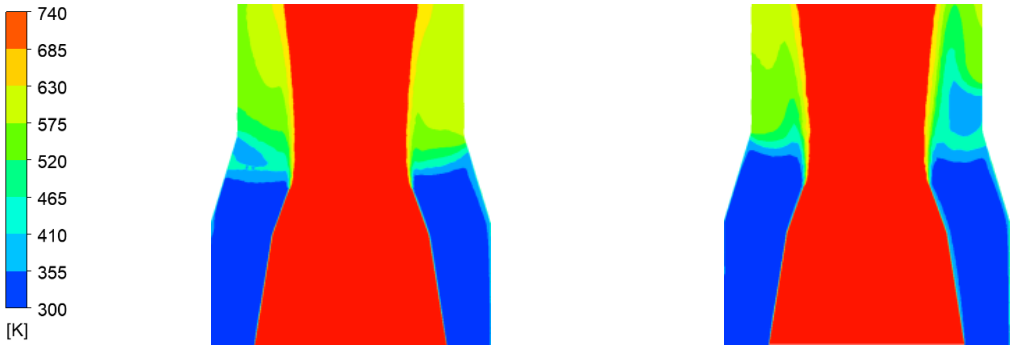

(a) $d = 80$ mm (b) $d = 160$ mm

Fig. 18 Temperature distributions with different lobed nozzle widths

In summary, increasing the lobed nozzle width decreases the EC, but on the positive side it also decreases the PLC and relieves the temperature rising inside the enclosure, caused by the high-temperature mainstream reflux.

3.1.3 Number of lobes

Different number of lobes n are compared and analyzed. 4 structures of lobes with n = 8, 10,12 and 14 are compared. Other structural parameters are $\alpha = 30°$, $d = 120$ mm, and $h = 630$ mm. The numerical simulation results are shown in Table 6.

Table 6 Numerical simulation results for different number of lobes

Structure	P_1 (Pa)	P_2 (Pa)	q (Pa)	EC	PLC
8	2036.544	4342.777	213.1120	0.2352	10.8217
10	2059.712	4269.302	210.9020	0.2191	10.4769
12	2063.709	4263.774	211.0914	0.2058	10.4223
14	2076.702	4235.984	210.9599	0.1904	10.2355

As shown in Table 6, the EC decreases from 0.2352 to 0.1904 and the PLC decreases from 10.8217 to 10.2355 when the number of lobes is increased from 8 to 14. It is worth noting that the fluctuation in pressure is within a small range. The expansion of the secondary fluid mixing area with fewer nozzles, leading to higher mainstream flow rates. This enhances secondary fluid entrainment, consequently leading to an increase in EC. However, this also leads to an increase in pressure loss since the number of recessed indentations in the nozzle also increases. Fig. 19 shows the pressure description at the nozzle outlet for different nozzle numbers.

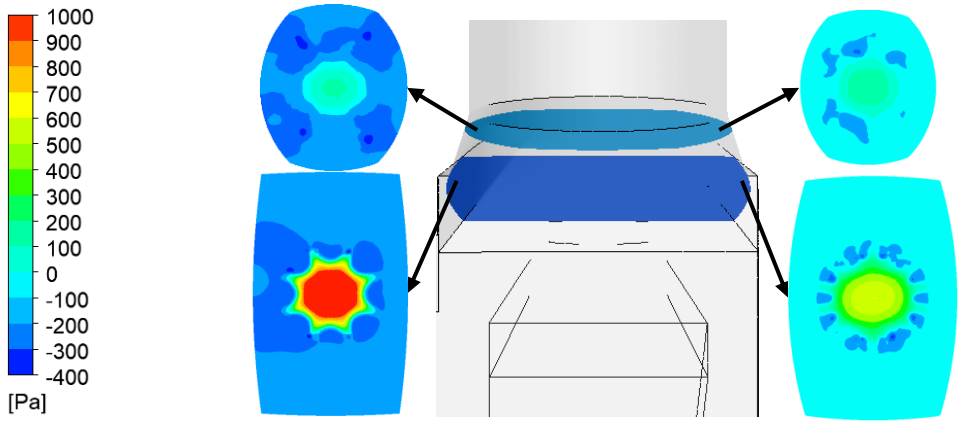

(a) $n = 8$ (b) $n = 14$

Fig. 19 Pressure distributions with different number of lobes

As shown in Fig. 19, when the number of nozzles is increased from 8 to 14, the negative pressure zone is weakened, so the ejection capability is reduced and the EC decreases significantly. The temperature

variation around the ejector outlet can well validate this conclusion. Fig. 20 shows the temperature inside the mixing tube at different number of lobes.

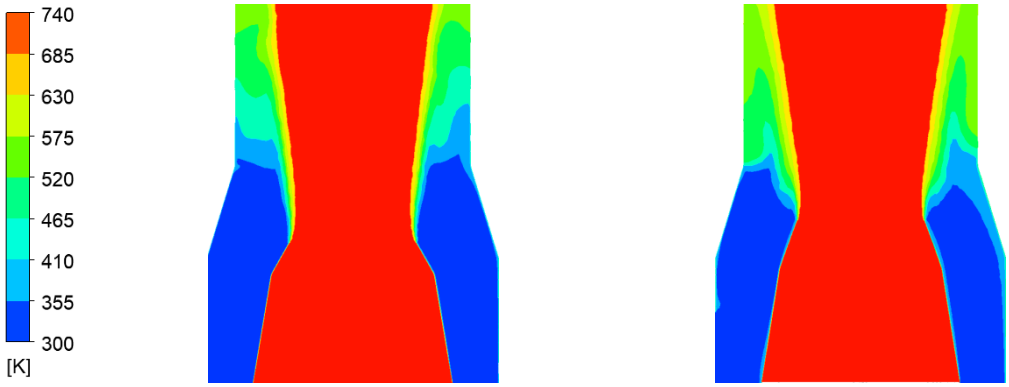

(a) $n = 8$ (b) $n = 14$

Fig. 20 Temperature distributions with different lobed nozzle widths

As shown in Fig. 20, a decrease in EC correlates with a reduced effectiveness of the ejection cooling process, especially in the region adjacent to the wall.

3.1.4 Height of square-to-circle

This section compares and analyses different square-to-circle section heights h. Five structures of the ejector are compared with $h = 570$ mm, 600 mm, 630 mm, 660 mm, and 690 mm. Other structural parameters are $\alpha = 30°$, $n = 10$, and $d = 120$ mm. The numerical simulation results are shown in Table 7.

Table 7 Numerical simulation results for different height of square-to-circle

Structure	P_1 (Pa)	P_2 (Pa)	q (Pa)	EC	PLC
570 mm	2122.172	4682.795	209.870	0.2302	12.2010
600 mm	2115.159	4616.049	210.107	0.2300	11.9029
630 mm	2059.712	4269.302	210.902	0.2191	10.4769
660 mm	2120.324	4556.828	210.398	0.2214	11.5804
690 mm	2119.225	4509.766	210.552	0.2219	11.6537

As can be seen from Table 7, both EC and PLC show a decreasing and then increasing trend with a small range of variation. The h will affect the position of the lobed nozzle outlet, lower-lobed nozzle outlet surface will promote mixing between the mainstream and secondary fluids, providing more space. Further into the outer square rotating circle will compress the secondary flow recirculation area, but to enhance the velocity as a compensation, as shown in Fig. 21. So that the EC and PLC tends to decrease and then increase, and the reason for a smaller range of fluctuation is that the flow field does not undergo a large change.

Fig. 22 presents temperature variations in the crest and trough sections for various values of h. Fig. 22 shows that changing h has a greater effect on the crest outlet of the lobed nozzle. This is attributed to the fact that as the nozzle outlet continually approaches the inlet of the mixing tube, the edge of the main stream is affected by the viscous effects of the secondary flow. This leads to a separation of the high-temperature gases, which impinge on the surface of the outer square-to-circle, and partly occur in the reflux and vortex within the inner part of the enclosure. When the nozzle outlet height exceeds this critical value, so that the high-temperature mainstream completely rushed into the mixing tube, this reflux heating phenomenon has been alleviated.

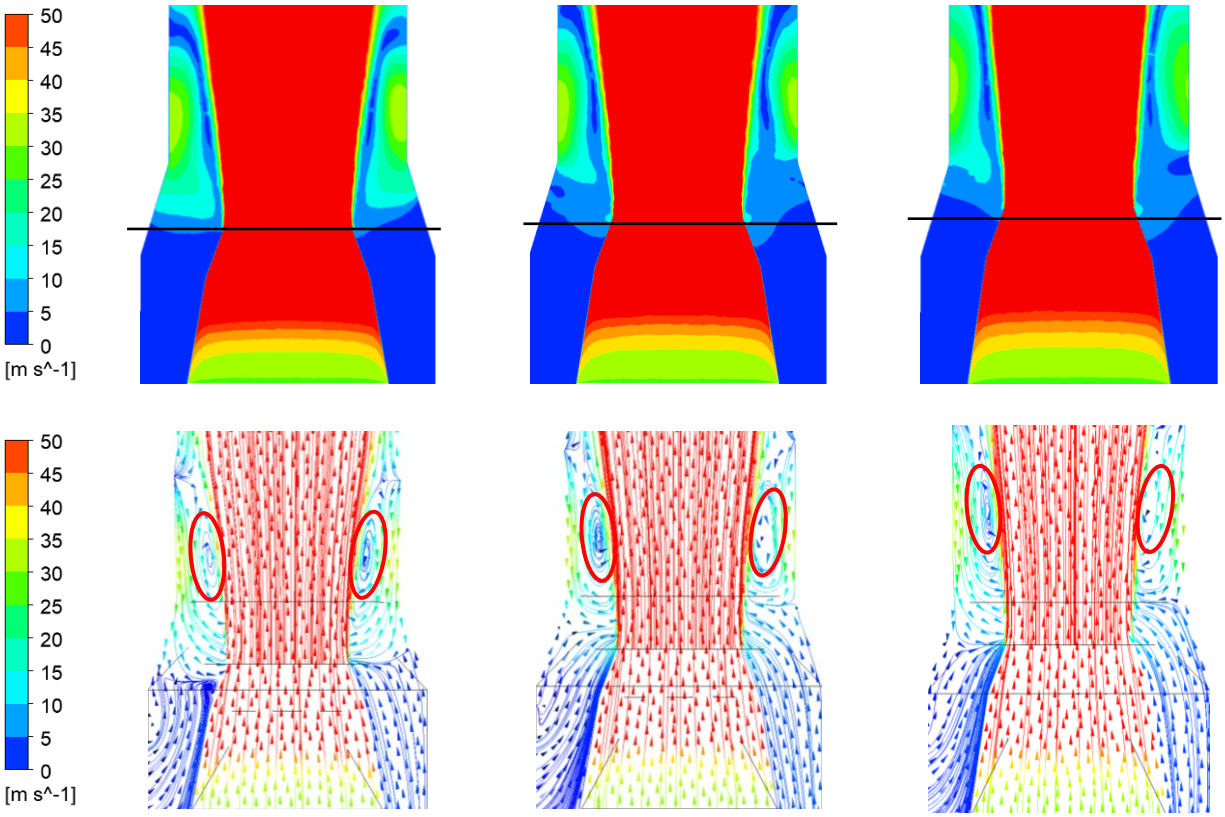

(a) h = 570 mm (b) h = 630 mm (c) h = 690 mm

Fig. 21 Velocity distributions with different height

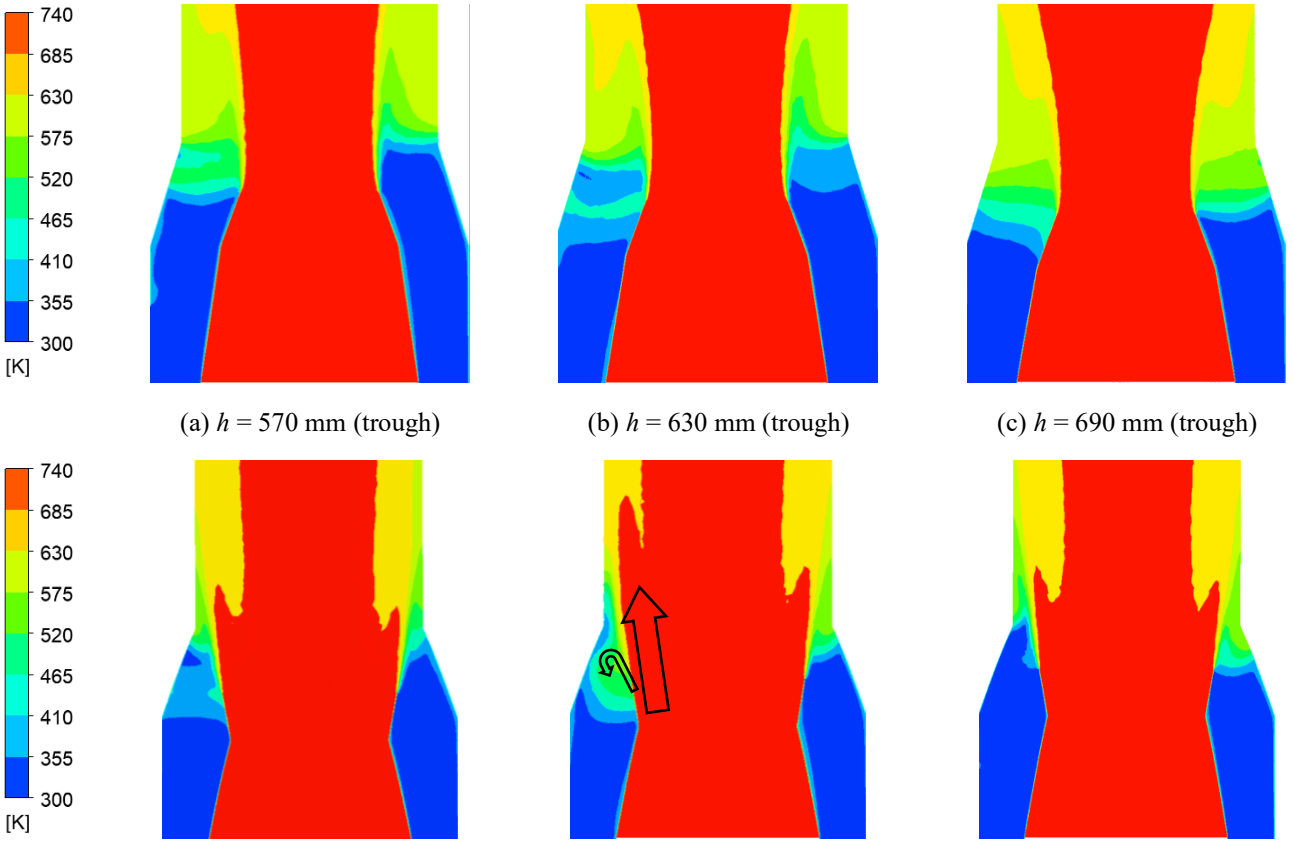

(a) h = 570 mm (trough) (b) h = 630 mm (trough) (c) h = 690 mm (trough)

(d) h = 570 mm (crest) (e) h = 630 mm (crest) (f) h = 690 mm (crest)

Fig. 22 Different temperature distributions in the crest and trough sections

3.2 Orthogonal test

Orthogonal parameter designs were calculated for the four structural variables studied in section 3.1, as shown in Table 8. The orthogonal table for the orthogonal tests conducted in this study and the numerical simulation results for each test are shown in Table 9.

Table 8 Designed parameters

Objects	Parameters			
Lobed expansion angle α	30°	35°	40°	45°
Lobed width d	100 mm	120 mm	140 mm	160 mm
Number of lobes n	8	10	12	14
Ejector outlet heights h	600 mm	630 mm	660 mm	690 mm

Table 9 Numerical simulation results

Number	A	B	C	D	Combination	EC	PLC
1	1	1	1	1	$A_1B_1C_1D_1$	0.2722	13.1094
2	1	1	2	2	$A_1B_1C_2D_2$	0.2404	11.4095
3	1	2	3	4	$A_1B_2C_3D_4$	0.1676	8.8524
4	1	2	4	3	$A_1B_2C_4D_3$	0.1878	10.1315
5	1	3	1	3	$A_1B_3C_1D_3$	0.2464	10.4957
6	1	3	2	4	$A_1B_3C_2D_4$	0.1893	8.8382
7	1	4	3	2	$A_1B_4C_3D_2$	0.1962	10.3238
8	1	4	4	1	$A_1B_4C_4D_1$	0.2468	10.5749
9	2	1	3	4	$A_2B_1C_3D_4$	0.2044	10.8959
10	2	1	4	3	$A_2B_1C_4D_3$	0.2196	11.9714
11	2	2	1	1	$A_2B_2C_1D_1$	0.2815	12.8011
12	2	2	2	2	$A_2B_2C_2D_2$	0.2281	11.2330
13	2	3	3	2	$A_2B_3C_3D_2$	0.2292	11.0725
14	2	3	4	1	$A_2B_3C_4D_1$	0.2548	10.6815
15	2	4	1	3	$A_2B_4C_1D_3$	0.2471	11.3831
16	2	4	2	4	$A_2B_4C_2D_4$	0.2080	9.2625
17	3	1	3	1	$A_3B_1C_3D_1$	0.2523	13.0819
18	3	1	4	2	$A_3B_1C_4D_2$	0.2433	13.3114
19	3	2	1	4	$A_3B_2C_1D_4$	0.2766	12.6187
20	3	2	2	3	$A_3B_2C_2D_3$	0.2464	11.6713
21	3	3	3	3	$A_3B_3C_3D_3$	0.2245	10.7923
22	3	3	4	4	$A_3B_3C_4D_4$	0.2101	9.1533
23	3	4	1	2	$A_3B_4C_1D_2$	0.2851	14.2300
24	3	4	2	1	$A_3B_4C_2D_1$	0.2636	12.6445
25	4	1	1	4	$A_4B_1C_1D_4$	0.2187	11.8308
26	4	1	2	3	$A_4B_1C_2D_3$	0.2454	12.0495
27	4	2	3	1	$A_4B_2C_3D_1$	0.2897	14.2007
28	4	2	4	2	$A_4B_2C_4D_2$	0.2600	14.2256
29	4	3	1	2	$A_4B_3C_1D_2$	0.2517	11.5837
30	4	3	2	1	$A_4B_3C_2D_1$	0.2818	10.7054
31	4	4	3	3	$A_4B_4C_3D_3$	0.2447	11.0572
32	4	4	4	4	$A_4B_4C_4D_4$	0.2540	11.2272

3.3 Multi-objective evaluation based on CRITIC method

To further increase the number of samples and improve the optimization-seeking accuracy, the genetic aggregation algorithm in WORKBENCH response surface analysis was used to predict the above numerical simulation results, and finally, 5000 results for different structures were obtained. In the following section, the CRITIC weighting method will be used to analyze the weights of two evaluation metrics.

The CRITIC weighting method is an objective weight assignment method proposed by Diakoulaki [37]. It utilizes the variability and conflict of evaluation metrics to comprehensively measure the objective weight of metrics [38]. This method is particularly suitable for multi-attribute and multi-objective decision-making scenarios. The steps of the integrated model construction of the CRITIC weighting method are as follows:

1. Suppose there are n samples for evaluation, each assessed using m evaluation metrics. This forms a raw data matrix of the evaluation metrics:

$$X = \begin{pmatrix} x_{11} & \cdots x_{1m} \\ \vdots & \ddots \vdots \\ x_{n1} & \cdots x_{nm} \end{pmatrix}, \tag{3}$$

The notation x_{ij} represents the value of the j-th evaluation metric for the i-th sample in the original data matrix, which consists of n samples and m evaluation metrics.

2. As the evaluation matrix PLC in this study is as small as possible. Therefore, the PLC matrix is reversed and normalized:

$$x_{ij}^{'} = \frac{x_{\max} - x_j}{x_{\max} - x_{\min}}, \tag{4}$$

3. The variability of matrices is expressed in the form of standard deviation:

$$\begin{cases} \overline{x}_j = \dfrac{1}{n}\sum_{i=1}^{n} x_{ij} \\ S_j = \sqrt{\dfrac{\sum_{i=1}^{n}\left(x_{ij} - \overline{x}_j\right)^2}{n-1}} \end{cases}, \tag{5}$$

where S_j shows the standard deviation of the j-th matrix.

4. Conflict of matrices is expressed by correlation coefficient:

$$R_j = \sum_{i=1}^{p}\left(1 - r_{ij}\right), \tag{6}$$

where r_{ij} denotes the correlation coefficient between evaluation matrices i and j.

5. Amount of information:

$$C_j = S_j \sum_{i=1}^{p}\left(1 - r_{ij}\right) = S_j \times R_j, \tag{7}$$

where the larger C_j is, the greater the role of the j-th evaluation matrix in the overall evaluation matrix system, and the more weight should be assigned to it.

6. Objective weights:

In summary, the objective weights W_j of the j-th matrix are:

$$W_j = \frac{C_j}{\sum_{j=1}^{p} C_j}, \tag{8}$$

This section uses the CRITIC evaluation method to perform a multi-objective comprehensive evaluation of the calculated results. The evaluation results of the CRITIC evaluation method are shown in Table 10 and found the optimal structural parameters on this basis, due to the limitation of space, this study takes the top 5 and last 5 solutions as examples, and the specific optimization results are shown in Table 11.

Table 10 Calculation results of the weights

Evaluation Metrics	Variability of indicators	Conflicting indicators	Information volume	Weight (W_j)
EC	0.193	1.82	0.351	49.38%
PLC	0.198	1.82	0.36	50.62%

Table 11 Predictive results of CRITIC method

NO	α	d	n	h	EC	PLC	SCORE
1	**45**	**150**	**14**	**600**	**0.2816**	**10.8141**	**0.7778**
2	44.375	150	8	600	0.2846	10.9603	0.7581
3	30	155	14	600	0.2797	10.8456	0.7578
4	43.125	150	8	600	0.2773	10.8985	0.7483
5	41.875	150	8	600	0.2763	10.8664	0.7353
4996	30	105	8	622.5	0.2608	14.3191	0.4006
4997	30	100	12	626.25	0.2492	13.7802	0.4001
4998	30	100	10	626.25	0.2577	14.1918	0.3991
4999	30	100	11	626.25	0.2510	13.9246	0.3952
5000	30	100	11	626.25	0.2538	14.0642	0.3947

As can be seen from Table 11, after the evaluation of the CRITIC method, the structure of the optimal solution with $\alpha = 45°$, $d = 150$ mm, $n = 14$, $h = 600$, where the EC reaches 28.16% and the PLC is only 10.8141. The overall score reaches 0.7778.

3.4 Validation of optimization results

The multi-objective evaluation is performed by CRITIC method, and the optimal solution is obtained. The optimal solution obtained from the prediction is verified by numerical simulation. A comparison of the results is shown in Table 12.

Table 12 Validation results of numerical simulations

NO	α	d	n	h	EC	PLC
Initial Model	30	120	10	630	0.2143	10.8642
Optimization Results	45	150	14	600	0.2816	10.8141
Numerical Simulation Validation	45	150	14	600	0.2798	10.6800

As can be seen from Table 12, the optimized structure well improves the EC while reducing the PLC, comparing the Optimization Results and Numerical Simulation Validation, the EC error is 0.6% and the PLC error is 1.2%, which verifies the accuracy of the genetic aggregation algorithm while further ensuring that the effectiveness of the optimized structure. A comparative analysis of the flow field and temperature distribution inside the enclosure assembly is performed and the initial lobed nozzle ejector to verify whether the temperature meets the design requirements. Fig. 23 shows the temperature distribution of a typical section within the gas turbine enclosure, and Fig. 24 shows the flow depiction of the exhaust system.

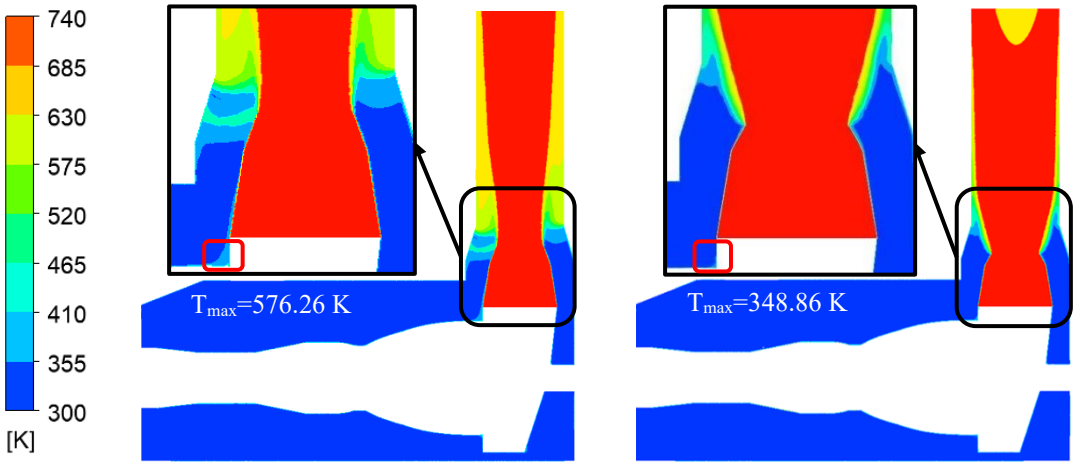

(a) Temperature distribution of initial model

(b) Temperature distribution of optimization results

Fig. 23 Temperature distribution of typical section

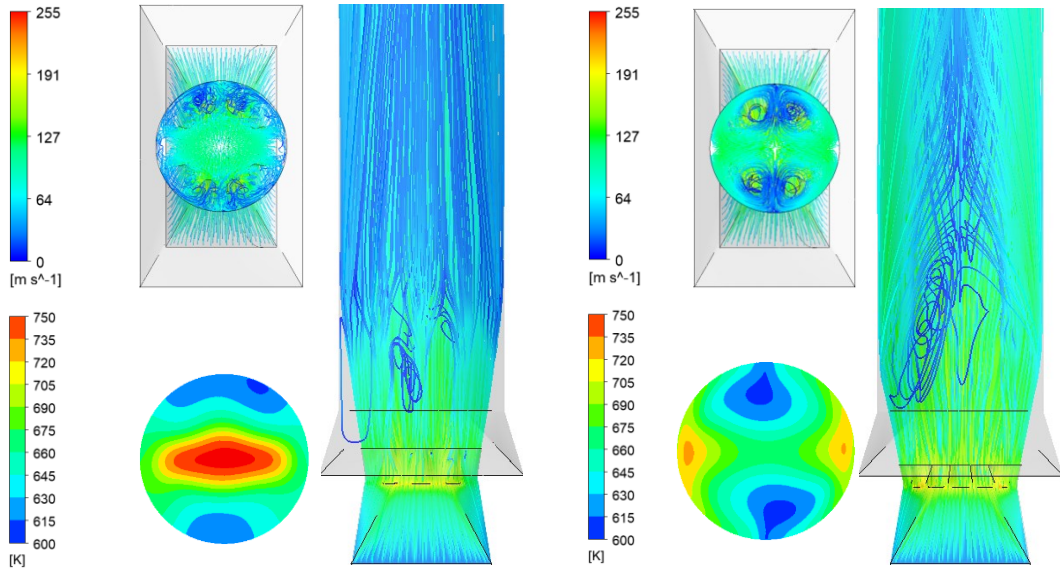

(a) Flow field of initial lobed nozzle ejector

(b) Flow field of optimized lobed nozzle ejector

Fig. 24 The flow depiction of the exhaust system

From Fig. 23, it's evident that the temperature surrounding the nozzle outlet is notably high. Furthermore, Fig. 24 highlights a significant issue prior to optimization: a pronounced high-temperature mainstream refluxing into the interior of the enclosure within the mixing tube. This design leads to inadequate mixing, with the high-temperature mainstream still concentrated predominantly in the middle of the tube. Additionally, the vortex edges are small and dispersed, failing to effectively reduce the temperature of both the high-temperature mainstream and the ejected secondary stream upon mixing.

Fig. 24(b) demonstrates the substantial improvements post-optimization. The temperature around the nozzle noticeably decreases, and the reflux within the mixing tube undergoes improvement. Moreover, the fluid flow evolves to form four symmetric and complete vortices, significantly boosting doping efficiency while reducing both the temperature and temperature differential of the exhaust gas. Notably, the maximum temperature at the typical cross-section inside the enclosure drops from 576.26 K to 348.86 K, meeting the design requirement of maintaining temperatures below 355 K.

4. Conclusion

This study aims to achieve an optimized design of the exhaust ejection ejector for marine gas turbines by investigating the impact of structural parameters of the lobed nozzle ejector to obtain a high-performance

configuration. Parameters such as lobed nozzle expansion angle (α), lobed nozzle width (d), number of lobes in the nozzle (n), and height of the square-to-circle section (h) are analyzed. An orthogonal experimental design is employed for this purpose. Subsequently, the CRITIC method is utilized for multi-objective evaluation to determine the optimal design structure for the lobed nozzle ejector.

(1) To validate the reliability of the turbulent model, an ejection characteristic testing system equipped with a convergent nozzle ejector was designed and constructed. Comparative analysis between experimental results and numerical simulations revealed that the Realizable k-ε model accurately simulated the actual velocity, with an absolute error rate of 6.23%.

(2) The lobed nozzle ejector can achieve a larger ejection coefficient (EC) while maintaining a low-pressure loss coefficient and preserving the overall pressure at the exhaust ejector outlet. Among the four parameters, the ejection coefficient (EC) and the pressure loss coefficient (PLC) are most significantly influenced by the lobed expansion angle α, and least affected by square-to-circle section heights h. However, if h is too small, it can cause the high-temperature mainstream reflux into the enclosure

(3) According to the CRITIC method, the weight (W_j) of the pressure loss coefficient (50.62%) is slightly higher than the ejection coefficient (49.38%). Applying the CRITIC method, the optimal solution is obtained corresponding to a lobed nozzle expansion angle α = 45°, lobed nozzle width d = 150 mm, number of the lobed nozzle n =14, height of the square-to-circle section h = 600 mm. The maximum temperature of the typical cross section inside the enclosure is reduced from 576.26 K to 348.86 K.

REFERENCES

[1] Ammar, N. R., Farag, A. I., 2016. CFD modeling of syngas combustion and emissions for marine gas turbine applications. *Polish Maritime Research*, 23(3), 39-49. https://doi.org/10.1515/pomr-2016-0030

[2] Cherednichenko, O., Serbin, S., Dzida, M., 2019. Application of thermo-chemical technologies for conversion of associated gas in diesel-gas turbine installations for oil and gas floating units. *Polish Maritime Research*, 26(3), 181-187. https://doi.org/10.2478/pomr-2019-0059

[3] Rasoulimoghadam, M., Kheradmand, S., 2019. Design and Numerical Simulation of the Performance of Acoustic Plenum Chamber of a Marine Gas Turbine Air Supply System. *Archives of Acoustics*, 44(4), 793-806.

[4] Domachowski, Z., Dzida, M., 2019. Applicability of inlet air fogging to marine gas turbine. *Polish Maritime Research*, 26(1), 15-19. https://doi.org/10.2478/pomr-2019-0002

[5] Dai, Y. F., Gao, C., Li, B., 2023. Assessment of the effectiveness of ventilation for gas turbine generator set safety. *Proceedings of the Institution of Mechanical Engineers, Part A: Journal of Power and Energy*, 237(5), 2025-224. https://doi.org/10.1177/09576509231153982

[6] Ma, L., Xu, T., Zhang, T. Y., Yu, Z. L., Guo, H. T., 2019, Heat Transfer Design for Bionic Surfaces in a Simplified Transition Segment of Marine Gas Turbine Combustor. *Tehnički Vjesnik-Technical Gazette*, 26(3), 722-727. https://doi.org/10.17559/TV-20190104103801

[7] Varga, S., Oliveira, A. C., Diaconu, B., 2009. Influence of geometrical factors on steam ejector performance - A numerical assessment. *International Journal of Refrigeration-Revue Internationale Du Froid*, 32(7), 1694-1701. https://doi.org/10.1016/j.ijrefrig.2009.05.009

[8] Sun, T., Liu, N., Wang, Z. Y., Ye, N., 2014. Numerical Simulation on the Controllable Two Stage Exhaust Ejector of Gas Turbine. *Journal of the Chinese Society of Mechanical Engineers*, 35(5), 397-404.

[9] Sun, T., Ye, N., Xu, Y. H., Wang, G. H., Yuan, M. H., 2015. Study of New Exhaust Ejector for Marine Gas Turbine. *Journal of Engineering for Gas Turbines and Power-Transactions of the ASME*, 137(12), 121505. https://doi.org/10.1115/1.4030516

[10] Jiang, K., Lu, X. Y., Wang, H., 2022. Influence of multiple structural parameters on buffer performance of a thin-walled circular tube based on the coupling modeling technique. *International Journal of Mechanical System Dynamics*, 2, 374-390. https://doi.org/10.1002/msd2.12060

[11] Padhi, A., Dash, S. K., 2022. Shape effect on natural convection heat transfer over a constant surface area vertical hollow frustum. *International Communications in Heat and Mass Transfer*, 138, 106373. https://doi.org/10.1016/j.icheatmasstransfer.2022.106373

[12] Vahidi, D., Bagheri, H., Glezer, B., 2006. Numerical and Experimental Study of Ventilation for Gas Turbine Package Enclosure. *ASME Turbo Expo 2006: Power for Land, Sea, and Air*, 8–11 May, Barcelona, Spain, 5, 607-616. https://doi.org/10.1115/GT2006-90960

[13] Lucherini, G., Minotti, S., Ragni, G., Bologna, F., 2018. Experimental and Numerical Investigation on Gas Turbine Package Scale Model. *ASME Turbo Expo 2018: Turbomachinery Technical Conference and Exposition*, 11–15 June, Oslo, Norway, 9, V009T27A018. https://doi.org/10.1115/GT2018-75694

[14] Kowalski, J., Mare, F. d., Theis, S., Wiedermann, A., Lange, M., and Mailach, R., 2019. Investigation of the ventilation flow in a gas turbine package enclosure. *13th European Conference on Turbomachinery Fluid Dynamics and Thermodynamics*, 8-12 April, Lausanne, Switzerland, ETC2019-438. https://doi.org/10.29008/ETC2019-438

[15] Birk, A. M., Davis, W. R., 1989. Suppressing the Infrared Signatures of Marine Gas Turbines. *Journal of Engineering for Gas Turbines and Power*, 111(1), 123-129. https://doi.org/10.1115/1.3240210

[16] Maqsood, A., Birk, A. M., 2005. Experimental and CFD Study of Exhaust Ejectors with Bent Mixing Tubes. *ASME Turbo Expo 2005: Power for Land, Sea, and Air*, 6-9 June, Reno, Nevada, USA, 1, 155-165. https://doi.org/10.1115/GT2005-68597

[17] Maqsood, A., Birk, A. M., 2007. Effect of a Bend on the Performance of an Oblong Ejector. *ASME Turbo Expo 2007: Power for Land, Sea, and Air*, 14-17 May, Montreal, Canada, 6, 37-45. https://doi.org/10.1115/GT2007-27851

[18] Maqsood, A., Birk, A. M., 2010. Effect of Entraining Diffuser on the Performance of Bent Exhaust Ejectors. *ASME Turbo Expo 2010: Power for Land, Sea, and Air*, 14-18 June, Glasgow, UK, 7, 2793-2802. https://doi.org/10.1115/GT2010-23499

[19] Maqsood, A., Birk, A. M., 2017. Wall Pressure and Temperature Distribution in Bent Oblong Exhaust Ejectors. *ASME Turbo Expo 2017: Turbomachinery Technical Conference and Exposition*, 26-30 June, Charlotte, North Carolina, USA, 2B, V02BT42A003. https://doi.org/10.1115/GT2017-63250

[20] Hu, H., Saga, T., Kobayashi, T., Taniguchi, N., 2000. Research on the vortical and turbulent structures in the lobed jet flow using laser induced fluorescence and particle image velocimetry techniques. *Measurement Science and Technology*, 11, 698-711. https://doi.org/10.1088/0957-0233/11/6/313

[21] Hu, H., Saga, T., Kobayashi, T., Taniguchi, N., 2001. A study on a lobed jet mixing flow by using stereoscopic particle image velocimetry technique. *Physics of Fluids*, 13, 3425-3441. https://doi.org/10.1063/1.1409537

[22] Hu, H., Saga, T., Kobayashi, T., Taniguchi, N., Yasuki, M., 2001. Dual-plane stereoscopic particle image velocimetry: system set-up and its application on a lobed jet mixing flow. *Experiments in Fluids*, 31, 277-293. https://doi.org/10.1007/s003480100283

[23] Năstase, I., Meslem, A., 2007. Passive control of jet flows using lobed nozzle geometries. *Mecanique & Industries*, 8, 101-109. https://doi.org/10.1051/meca:2007027

[24] Paul, R. V., Kriparaj, K. G., Tide, P. S., 2020. Numerical predictions of the flow characteristics of subsonic jet emanating from corrugated lobed nozzle. *Aircraft Engineering and Aerospace Technology*, 92, 955-972. https://doi.org/10.1108/AEAT-03-2019-0041

[25] Sheng, Z. Q., Wu, Z., Ji, J. Z., Huang, P. L., 2016. Chevron spoiler to improve the performance of lobed ejector/mixer. *International Communications in Heat and Mass Transfer*, 77, 174-182. https://doi.org/10.1016/j.icheatmasstransfer.2016.08.008

[26] Liu, D. W., Huang, J., Sheng, Z. Q., Ji, J. Z., 2016. The Effects of Spoilers on Jet Mixing of Lobed Nozzles. *Journal of Aerospace Technology and Management,* 4, 459-466. https://doi.org/10.5028/jatm.v8i4.606

[27] Sheng, Z. Q., Yao, Y. and Xu, Y. H., 2019. Suggestions on investigations of lobed jet mixing, *Aerospace Science and Technology*, 86, 415-429. https://doi.org/10.1016/j.ast.2019.01.042

[28] Shi, H., Zhang, Q. W., Liu, M. N., Yang, K. J., Yuan, J., 2022. Numerical Study of the Ejection Cooling Mechanism of Ventilation for a Marine Gas Turbine Enclosure. *Polish Maritime Research*, 29(3), 119-127. https://doi.org/10.2478/pomr-2022-0032

[29] Sheng, Z. Q., 2017. Jet mixing of lobed nozzles with spoilers located at lobe peaks. *Applied Thermal Engineering*, 119, 165-175. https://doi.org/10.1016/j.applthermaleng.2017.03.048

[30] Sheng, Z. Q., Huang, P. L., Zhao, T., Ji, J. Z., 2015. Configurations of lobed nozzles for high mixing effectiveness. *International Journal of Heat and Mass Transfer*, 91, 671-683. https://doi.org/10.1016/j.ijheatmasstransfer.2015.08.022

[31] Abdelmotalib, H. M., Lee, C.-E., Seo, Y., Lee, J., 2021. A computational study of two-dimensional serpentine nozzle performance with different annular mixer configurations. *International Journal of Mechanical Sciences*, 208, 106690. https://doi.org/10.1016/j.ijmecsci.2021.106690

[32] Shi, H., Zheng, R.T., Zhang, Q.W., Yuan, J., Wang, R., Cheng, M.M., Zou, Y.T., 2023. Numerical investigation of multi-nozzle ejector device with inclined nozzles for marine gas turbine. *Brodogradnja,* 74(4), 1-15. https://doi.org/10.21278/brod74401

[33] Shojaeefard, M. H., Ariafar, K., Goudarzi, K., 2009. Numerical investigation of flow in the liner of a model reverse-flow gas turbine combustor. *Proceedings of the Institution of Mechanical Engineers Part G: Journal of Aerospace Engineering,* 223(G8), 1083-1090. https://doi.org/10.1243/09544100JAERO537

[34] Bagheri, H., Vahidi, D., 2006. Ventilation of Gas Turbine Package Enclosures: Design Evaluation Procedure. *25th International Conference on Offshore Mechanics and Arctic Engineering*, 4-9 June, Hamburg, Germany, 1, 607-613. https://doi.org/10.1115/OMAE2006-92554

[35] Xiao, J., Wu, Q., Chen, L., Ke, W., Wu, C., Yang, X., Yu, L., Jiang, H., 2022. Assessment of Different CFD Modeling and Solving Approaches for a Supersonic Steam Ejector Simulation, *Atmosphere*, 13, 1. https://doi.org/10.3390/atmos13010144

[36] Sarkar, A., 2004. Experimental and numerical studies on performance of the air-air ejectors in confined spaces, Master Thesis, Queen's University, Kingston, Ontario, Canada.

[37] Hwang, S. N., Lee, H. S., Tang, S. C. and Hsu, S. S., 2013. Measuring Quality of Life Using DEA-AR: Focusing on Undesirable Factors, *Infor*, 51(2), 84-91. https://doi.org/10.3138/infor.51.2.84

[38] Krishnan, A. R., Kasim, M. M., Hamid, R., Ghazali, M. F., 2021. A Modified CRITIC Method to Estimate the Objective Weights of Decision Criteria. Symmetry-Basel, 13(6), 973. https://doi.org/10.3390/sym13060973